Topographic and BRDF Corrections for NEON Imaging Spectrometer-derived Reflectance Data

Algorithm Theoretical Basis Document

Shashi Konduri, Tristan Goulden

July 2023

1 Background

In the year 2020, the NEON AOP Sampling Design Technical Working Group (ASD TWG) reviewed all AOP data products for their overall quality, appropriateness of algorithms, and suitability of naming conventions. One of the key findings of the assessment was that the L1 (Level 1) spectrometer-derived directional reflectance (National Ecological Observatory Network (NEON), 2023) should be improved with the addition of a BRDF (Bi-directional reflectance distribution function) correction. The TWG members recommended that both the 'surface directional reflectance' products (i.e., no BRDF correction applied) and the 'surface bidirectional reflectance' products (BRDF corrected reflectance) be made available on the NEON data portal. The TWG also recommended the use of bidirectional surface reflectance for generating higher level (L2 and L3) data products such as vegetation indices, Leaf Area Index (LAI), Fraction of Photosynthetically Active Radiation (FPAR), and plant foliar traits, as these products would benefit from the BRDF correction.

2 Tasks

1. Apply topographic and BRDF corrections on the NEON Imaging Spectrometer (NIS)-derived reflectance data for a few NEON sites and share the corrected reflectance files with subject experts for their feedback.

2. Based on the feedback received, apply these corrections to the reflectance data collected for all the NEON sites flown in 2022 and 2023.

3. Retroactively apply these corrections to the already published surface directional reflectance data for all NEON sites and reprocess the L2 and L3 products for all previous years.

3 Need for corrections

3.1 Topographic correction

Steep mountain slopes can severely affect the remote sensing of vegetation. In areas with complex terrain, slopes facing the Sun receive more light and appear brighter than slopes facing away from the Sun (Figure 1). The irradiation on a slope varies strongly with the slope azimuth relative to

Figure 1: RGB image for the NEON Santa Rita Experimental Range (SRER) site. Differences in terrain orientation could cause variations in the reflectance values between pixels with similar land cover types and canopy structural properties (Image Source: Google Maps).

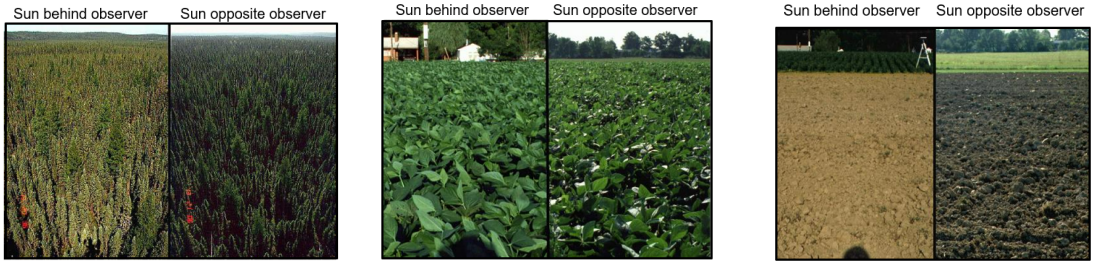

(a) Black Spruce Forest **(b)** Soybeans field **(c)** Barren field

Figure 2: Changes in the solar- and sensor view-angles could result in differences in the reflectance values recorded for different land cover types – **a)** Black Spruce Forest **b)** Soybeans field and **c)** Barren field. For each example case, the image on the left was taken with the sun behind the observer while the image on the right was taken with the sun opposite the observer. (Photographs by Donald W. Deering, NASA GSFC; Image source: https://www.umb.edu/spectralmass/terra_aqua_modis/modis).

the sun, and the reflectance of the slope varies with the angles of incidence and exitance relative to the slope normal. Topographic correction involves standardizing the imagery for these two effects based on the slope of the terrain and its relative position with the sun. (Shepherd & Dymond, 2003; Soenen, Peddle, & Coburn, 2005).

3.2 BRDF correction

Objects look differently when viewed from different angles, and when illuminated from different directions (Figure 2). The Bidirectional Reflectance Distribution Function (BRDF) describes the directional dependence of the reflected energy of a target as a function of the illumination and viewing geometry (Figure 3). BRDF depends on the wavelength of light and is determined by the surface structure and optical properties (Lucht et al., 2000). Surface structure influences BRDF through shadowcasting, mutual view shadowing, and spatial distribution of surface elements, such as the distribution of leaves inside plant canopy (Figure 4), while surface optical properties determine the BRDF through vegetation-soil contrasts and the optical attributes of canopy elements. Land surface albedo, an important parameter characterizing the earth's radiative regime, is related to land surface reflectance by directional integration and depends on the BRDF.

To reduce the effects of BRDF, the NEON Airborne Observation Platform (AOP) conducts aerial

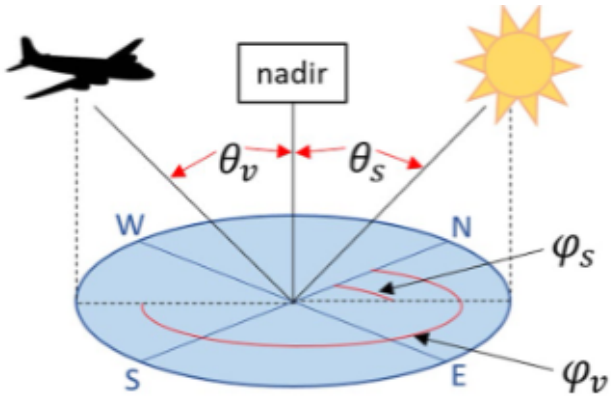

Figure 3: BRDF is a function of the view zenith angle (θ_v), solar zenith angle (θ_s) and relative azimuth angle between the sun and sensor ($\varphi_t = \varphi_s - \varphi_v$) (Image source: Queally et al. (2022)).

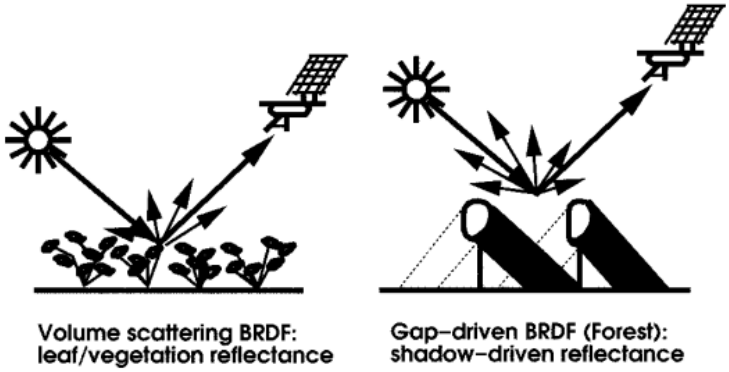

Figure 4: BRDF effects over vegetated areas result from a combination of radiative transfer-type volumetric scattering by leaves and geometric-optical surface scattering, which is given by shadowcasting and mutual obscuration of trees in a forest (Image source: Lucht et al. (2000)).

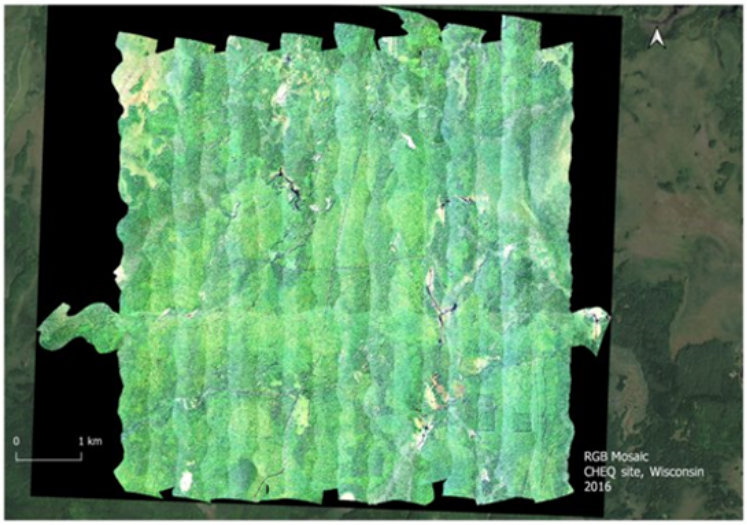

Figure 5: RGB mosaic created using directional reflectance data collected for 2016 for the NEON site in the Chequamegon (CHEQ) forest, Wisconsin. Variations in the relative position of the sun and sensor at the time of conducting aerial surveys can cause brightness gradients within and across flight lines in an image mosaic.

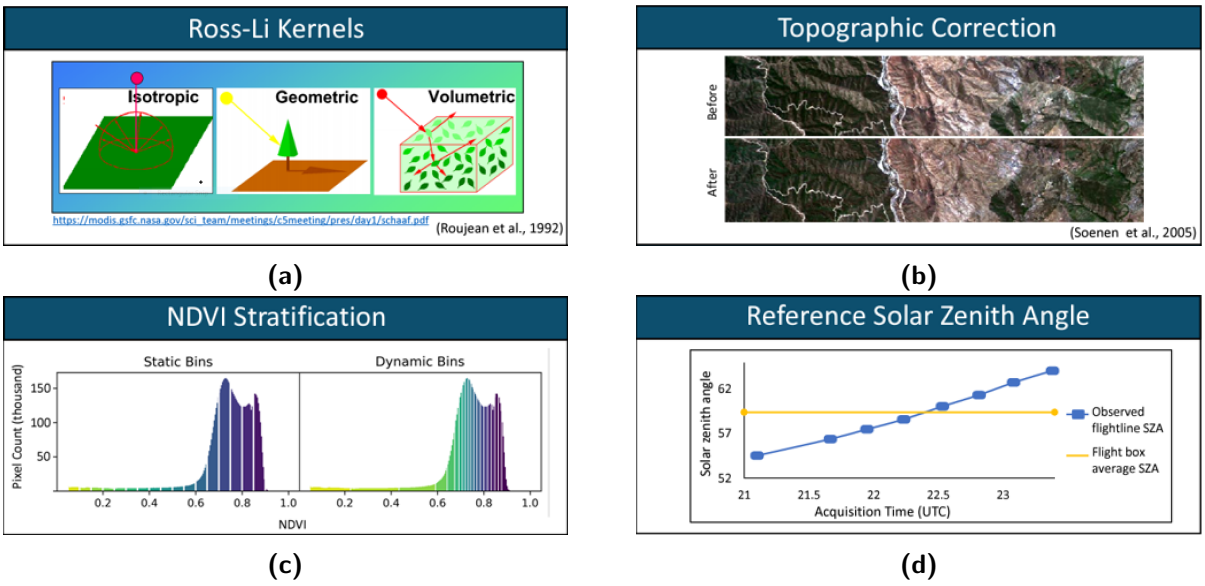

Figure 6: Summary of the FlexBRDF approach (Queally et al., 2022) for applying topographic- and BRDF-corrections on NEON airborne hyperspectral imagery. **a)** The BRDF correction routine uses semi-empirical kernels to capture diffuse radiation, tree shadows, and volumetric scattering by leaves. **b)** The topographic correction algorithm uses the $SCS + C$ method (Soenen et al., 2005) to correct for variations in reflectance due to terrain effects. **c)** BRDF effects depend on the vegetation type and structure. To account for this, the FlexBRDF approach stratifies pixels based on NDVI and estimates the BRDF coefficients (Equation 5) separately for each NDVI bin. **d)** To reduce brightness gradients within a mosaic, a reference solar zenith angle is calculated to standardize the reflectance observations collected under varying sun angles to a common standard.

surveys around solar noon (at a minimum solar elevation angle of 40^o) and in the North-South or South-North directions (Musinsky et al., 2022). Still, variations in solar and view geometry at the time of conducting aerial surveys can cause unwanted brightness gradients within and across flight lines in an image mosaic (Figure 5) that can confound scientific analyses (Colgan, Baldeck, Féret, & Asner, 2012; Queally et al., 2022). Correcting for BRDF effects involves adjusting the reflectance values on a per-pixel and per-wavelength basis to a standard view- (nadir) and solar angle, while accounting for differences in surface properties such as vegetation type and structure.

4 Methods

We followed the FlexBRDF approach (Queally et al., 2022) to correct for topographic- and BRDF-effects in the NEON reflectance data (Figure 6). This approach was selected for multiple reasons. First, this method was developed specifically for processing high-resolution airborne hyperspectral imagery. Second, this approach allows for the simultaneous processing of numerous flight lines, which helps remove brightness gradients across flight lines in an image mosaic. Third, these corrections were effective at various sites with diverse land cover types and terrain conditions. Lastly, the code to apply these corrections is available as an open-source Python package called HyTools (`https://github.com/EnSpec/hytools`).

4.1 Topographic Corrections

The FlexBRDF approach uses the $SCS + C$ method (Soenen et al., 2005) to correct for topographic effects in the reflectance data. Briefly, this method considers the Sun-Canopy-Sensor (SCS)

geometry to preserve the geotropic nature of trees (vertical growth), along with an additional C correction to account for an overcorrection problem in specific terrain orientations. (Soenen et al., 2005) showed this approach to be better than terrain-based corrections (cosine, C, Minnaert, and statistical-empirical) over a wide range of slopes, aspects, and crown closures in a Rocky Mountain forest setting in western Canada. The $SCS + C$ method corrects for the topography-induced brightness difference as a function of its slope (α), solar zenith angle (θ_s), and the relative azimuth angle between the Sun and terrain (φ_t).

$$R_t = R\frac{\cos\alpha\cos\theta_s + C}{\cos i + C} \tag{1}$$

where R_t and R are the topographically corrected reflectance and the uncorrected reflectance, respectively. $\cos i$ is the illumination factor and is calculated as:

$$\cos i = \cos\alpha\cos\theta_s + \sin\alpha\sin\theta_s\cos\varphi_t \tag{2}$$

and C is a function of the parameters of the linear relationship observed between R and $\cos i$,

$$R = a + b\cos i \quad and \quad C = \frac{a}{b} \tag{3}$$

The slope (α), solar zenith angle (θ_s), and the relative azimuth angle between the sun and terrain (φ_t) are provided as raster data and can be accessed from the metadata of the directional reflectance hdf5 files. The HyTools python package extracts the pixel-wise values of these angles from the hdf5 metadata to calculate the topographically-corrected reflectance (Equations 1-3) one pixel at a time.

4.2 BRDF correction

4.2.1 Kernels

FlexBRDF uses the approach proposed by (Roujean, Leroy, & Deschamps, 1992) to model BRDF as a linear sum of kernels (Equation 11). Semi-empirical kernel-based methods have been preferred over physics-based approaches for BRDF corrections due to their computational feasibility, scalability, and model parsimony (Roy et al., 2016; Schaaf et al., 2002). FlexBRDF uses a Ross-Li kernel-based approach to capture leaf-level scattering and tree shadows (Figure 6a). The Ross volumetric kernel describes the distribution of facets (i.e. leaves); the Ross-Thick kernel assumes the Leaf Area Index (LAI) ≥ 1, while Ross-Thin assumes $LAI < 1$. The geometric Li kernels describe the arrangement of trees in the landscape. The Li-sparse kernel is appropriate for sparse vegetation characterized by prominent shadows, whereas the Li-Dense kernel would suit dense vegetation. The complete mathematical formulation for the derivation of the geometric and volumetric kernels (K_{geo} and K_{vol}) follows (Wanner, Li, & Strahler, 1995):

$$K_{geo} = O - \sec\theta_s^{'} - \sec\theta_v^{'} + \frac{1}{2}(1+\cos\xi^{'})\sec\theta_v^{'} \tag{4}$$

$$K_{vol} = \frac{(\frac{\pi}{2}-\xi)\cos\xi + \sin\xi}{\cos\theta_s + \cos\theta_v} - \frac{\pi}{4}\xi \tag{5}$$

where

$$\theta^{'} = \tan^{-1}(\frac{b}{r}\tan\theta) \tag{6}$$

$$D = \sqrt{\tan^2\theta_s' + \tan^2\theta_v' - 2\tan\theta_s'\tan\theta_v'\cos\varphi} \tag{7}$$

$$\cos t = \frac{h}{b}\frac{\sqrt{D^2 + (\tan\theta_s'\tan\theta_v'\sin\varphi)^2}}{\sec\theta_s' + \sec\theta_v'} \tag{8}$$

$$O = \frac{1}{\pi}(t - \sin t\cos t)(\sec\theta_s' + \sec\theta_v') \tag{9}$$

$$\cos\xi' = \cos\theta_s'\cos\theta_v' + \sin\theta_s'\sin\theta_v'\cos\varphi \tag{10}$$

The fractions $\frac{b}{r}$ (Equation 6) and $\frac{h}{b}$ (Equation 8) are constants that describe the shape and height of the vegetation, respectively. Equations 6-10 are used to estimate K_{geo} (Equation 4) and K_{vol} (Equation 5). The K values are fixed values derived for each wavelength and are a function of each pixel's combination of view- and solar angles. The BRDF model, fitted separately for each wavelength band, is a linear regression between the observed reflectance (or, in this case, the topographically corrected reflectance) and the kernel values (K_{geo}, K_{vol}):

$$\rho(\theta_v, \theta_s, \varphi) = f_{iso} + f_{geo}K_{geo}(\theta_v, \theta_s, \varphi) + f_{vol}K_{vol}(\theta_v, \theta_s, \varphi) \tag{11}$$

Where f_{iso}, f_{geo}, and f_{vol} are the least square regression coefficients (henceforth referred to as BRDF coefficients) that describe a characteristic land cover type. The BRDF correction approximates nadir ($\theta_v = 0$) reflectance for each pixel based on the calculated kernel values and the derived BRDF coefficients. Equation 12 describes the application of the correction factors, which compare the observed reflectance of a pixel (in this case, the topographically corrected reflectance R_t) to the modeled reflectance at nadir. These factors are calculated and applied per wavelength band and pixel, outputting the topographic and BRDF-corrected reflectance R_{tb}.

$$R_{tb} = R_t(0, \theta_s, \varphi_n) = R_t(\theta_v, \theta_s, \varphi)\frac{\rho(0, \theta_s, \varphi_n)}{\rho(\theta_v, \theta_s, \varphi)} \tag{12}$$

4.2.2 NDVI-based stratification and Reference solar zenith angle

BRDF effects vary by surface type and structure. To account for differences in BRDF effects due to variations in vegetation type and structure, the FlexBRDF approach groups pixels based on normalized differenced vegetation index (NDVI) values (Figure 6c, Equation 13), and calculates the BRDF coefficients separately for each NDVI bin (Equation 11). To prevent the risk of abrupt boundaries in BRDF-corrected reflectance at the transitions between NDVI bins, BRDF coefficients are regressed to be continuous across NDVI bins rather than constant values for each bin.

$$NDVI = \frac{R_{850} - R_{665}}{R_{850} + R_{665}} \tag{13}$$

Where R_{850} and R_{665} are the directional reflectance values of the 850-nm and 665-nm bands, respectively. Conducting aerial surveys over a NEON site typically requires several hours of flying within a day, spread over multiple days depending on the weather conditions. When collecting data, the resulting variations in the sun angle introduce systematic line-to-line brightness differences. To account for this, FlexBRDF corrects all lines within a flight box with respect to a reference solar zenith angle (θ_{sr}), calculated as the average solar zenith angle across all flight lines within the flight box (Figure 6d).

Table 1: NEON sites chosen for testing the topographic- and BRDF-corrections

	NEON Domain	Site Name	Year	Dominant land cover type
1.	D03	Ordway-Swisher Biological Station (OSBS), Florida	2014	Herbaceous wetlands, Evergreen forest
2.	D05	Chequamegon Forest (CHEQ), Wisconsin	2017	Deciduous Forest, Mixed Forest
3.	D07	Great Smoky Mountains National Park (GRSM), Tennessee	2016	Deciduous Forest, Evergreen Forest
4.	D08	Talladega National Forest (TALL), Alabama	2015	Deciduous Forest, Evergreen Forest
5.	D14	Santa Rita Experimental Range (SRER), Arizona	2018	Shrub/scrub
6.	D17	Soaproot Saddle (SOAP), California	2021	Evergreen Forest, Shrub/scrub

4.3 Implementing the corrections

We followed the FlexBRDF approach to perform topographic- and BRDF-corrections on directional reflectance data (National Ecological Observatory Network (NEON), 2023) collected for multiple NEON sites with diverse land cover types (Table 1). The first step in the workflow (Figure 7 left) involves estimating the initial set of BRDF coefficients. For this step, a small fraction of pixels (10%) are sampled uniformly across all flight lines and corrected for topographic effects (Equations 1-3). The corrected pixels are then stratified based on their NDVI values, with the BRDF coefficients estimated separately for each NDVI bin and wavelength band (Equation 11). The next step in the workflow involves deploying the BRDF model for grouped processing of multiple flight lines to generate topographic- and BRDF-corrected reflectance data (Figure 7 right). The initial set of BRDF coefficients estimated in the model-fitting step are regressed across NDVI bins to avoid any sharp differences in brightness levels across NDVI bins. The grouped processing is performed using a reference solar zenith angle, calculated as the average of solar zenith angles for all lines within the box. Implementing the topographic corrections (Equations 1-3) is relatively straightforward, requiring information about just the topography (slope) and the solar and view geometry. BRDF corrections, however, require the user to provide values for various parameters that characterize the vegetation type, density, and structure (listed in Table 2).

Table 2: List of user-specified parameters and their values for performing Topographic- and BRDF-corrections. Parameter values were kept the same for all the sites.

Correction Type	Parameter Name	Definition	Value
Topographic	Method	Method for performing topographic correction: C, Cosine, SCS, SCS + C, Minneart	SCS + C (Soenen et al., 2005)

BRDF	Geometric Kernel (K_{geo})	Captures the geometric structure of reflectors and shadowing effects. "Li-Sparse" and "Li-Dense" are appropriate for sparse and dense vegetation.	Li-Sparse (Wanner et al., 1995)
	$\frac{b}{r}$	Characterizes vegetation shape in the geometric kernel	10 (Colgan et al., 2012)
	$\frac{h}{b}$	Characterizes vegetation height in the geometric kernel	2 (Colgan et al., 2012)
	Volumetric Kernel (K_{vol})	Captures leaf-scale volumetric scattering. "Ross-Thick" (LAI $>$ 1) and "Ross-Thin" (LAI $<$ 1).	Ross-Thick (Wanner et al., 1995)
	Percent sampled	Percentage of pixels sampled uniformly across all flight lines for fitting the BRDF model	10%
	Calc Mask	Pixels to exclude prior to **calculating (fitting)** the BRDF model. Masking can be performed based on topography (slope and aspect), clouds and cloud shadow detection, vegetation indices etc.	BRDF model was developed on pixels satisfying 0.1 $<$ NDVI $<$ 1 (water- and snow-covered pixels excluded). Cloud and cloud shadow masking was not performed.
	Apply Mask	Pixels to exclude when **applying** the BRDF model. Masking can be performed based on topography (slope and aspect), clouds and cloud shadow detection, vegetation indices etc.	BRDF model was applied on pixels satisfying 0.1 $<$ NDVI $<$ 1 (water- and snow-covered pixels excluded). Cloud and cloud shadow masking was not performed.
	# NDVI bins	Pixels are stratified based on NDVI before correction. BRDF coefficients are calculated separately for each NDVI bin.	18
	NDVI binning strategy	Static binning requires the user to provide the bin intervals. Dynamic binning automatically groups the pixels such that each bin has roughly the same number of pixels.	Dynamic binning

	Interpolation method	Method for interpolating BRDF coefficients across NDVI bins. This is done to reduce between-bin edges. Options include unweighted and weighted linear regression (weighted based on the size of the NDVI bin) and linear interpolation.	Linear interpolation
	Reference Solar Zenith Angle	The HyTools package provides different options for calculating the reference solar zenith angle.	Reference value for the entire flight box is calculated as the average solar zenith angle (θ_s) across all flight lines within the flight box.

5 Results

5.1 Topographic Correction

To evaluate topographic corrections, we selected two sites with complex terrain, the SRER site in AZ and the GRSM site in TN. While the correction seems to be effective for the SRER site with a noticeable reduction in the differences between reflectance values on either side of the ridge line (Figure 8), the correction does not seem to be as effective for the GRSM site (Figure 9).

5.2 BRDF correction

The BRDF-corrected flight lines were evaluated qualitatively by inspecting the RGB mosaics for clear boundaries between flight lines. A seamless-looking RGB mosaic devoid of brightness gradients indicates a good BRDF correction. In addition to performing a visual comparison, we compared the pixel values between overlapping areas of adjacent flight lines to assess spectral consistency. Specifically, we calculated the Root Mean Squared Error (RMSE) between reflectance values from the overlapping areas of several pairs of adjacent flight lines as a quantitative metric to determine the goodness of correction. RMSE values were compared across all wavelength bands (except for wavelength regions affected by water vapor absorption). Figures 10-15 provide a visual comparison of the RGB mosaics and a quantitative comparison of the reflectance values from adjacent flight lines before and after applying the topographic and BRDF corrections for each of the six NEON sites. We also tested the corrections on flight lines collected in a star formation for the CPER site, CO, in 2020 (Figure 16).

Our results show that the corrections seem to be effective for sites dominated by open cover types, such as the OSBS site, Florida (herbaceous wetlands), the SRER site, Arizona (shrub/scrub cover), SOAP site, California (forest cover mixed with shrubs) and CPER site, Colorado (Grassland/Herbaceous). On the other hand, NEON sites dominated by dense forest cover, such as the CHEQ site in Wisconsin and the GRSM site in Tennessee, show a slight reduction in the brightness gradients across flight lines post-correction. For the GRSM site, varying the values of parameters did not improve the RMSE. Specifically, we tested various combinations of the Ross volumetric kernels (Thick/Thin) and Li geometric kernels (Dense/Sparse) and varied the number of NDVI bins between 3 and 18 (Figure 17).

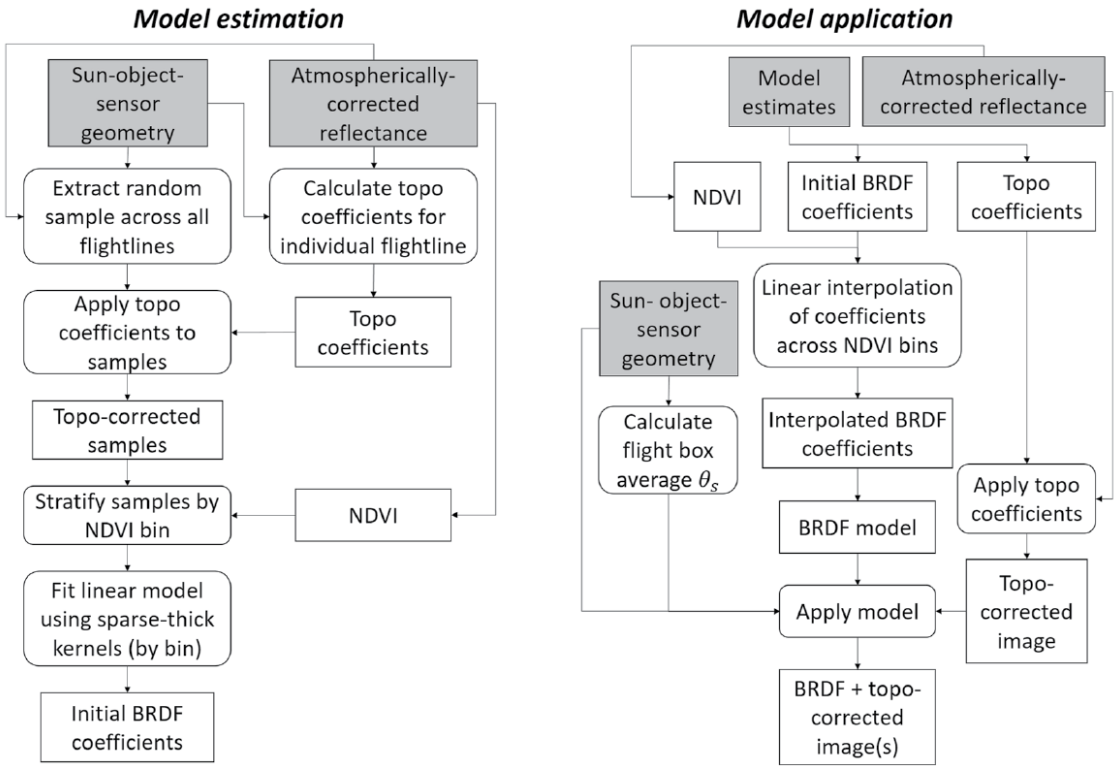

Figure 7: The FlexBRDF workflow consists of a model-fitting step (left), which involves estimating the initial set of BRDF coefficients using a small fraction of pixels sampled uniformly across all flight lines, followed by a model deployment step (right), which involves interpolating the BRDF coefficients across NDVI bins for grouped processing of multiple flight lines to generate topographic- and BRDF-corrected reflectance data (Image source: (Queally et al., 2022)).

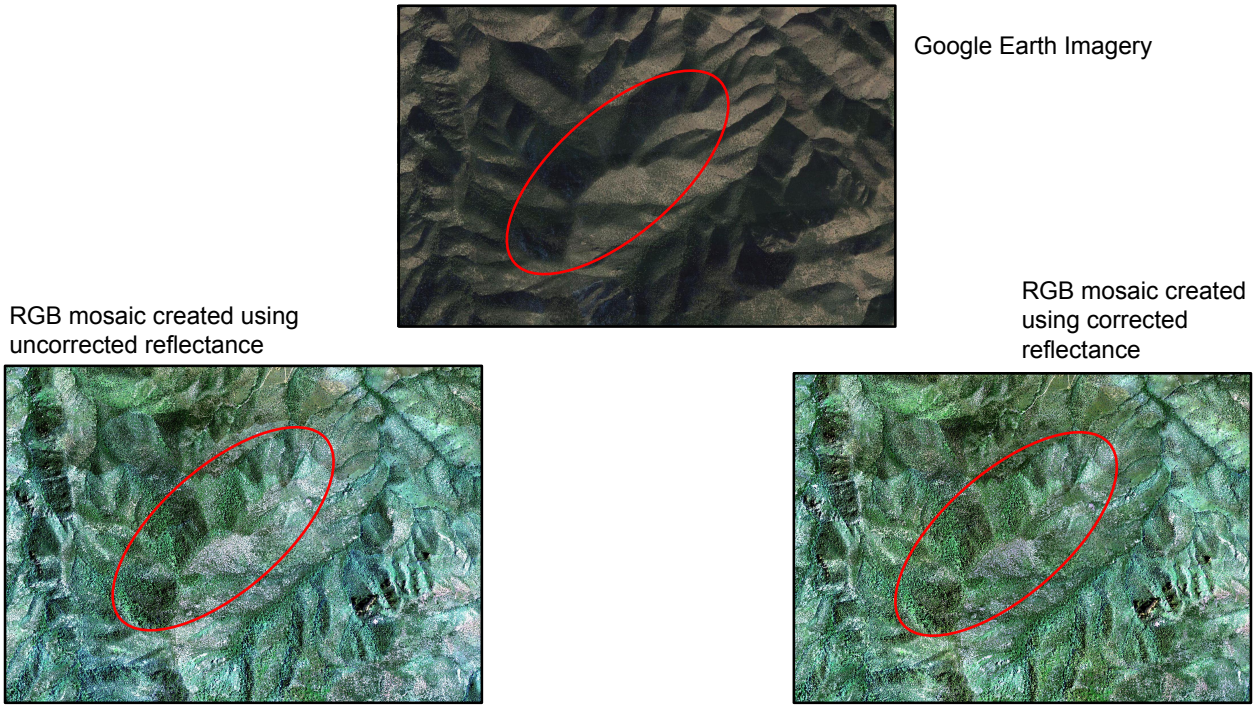

Figure 8: Topographic correction on the uncorrected reflectance for the SRER site, AZ reduced the differences between reflectance values on either side of the ridge line.

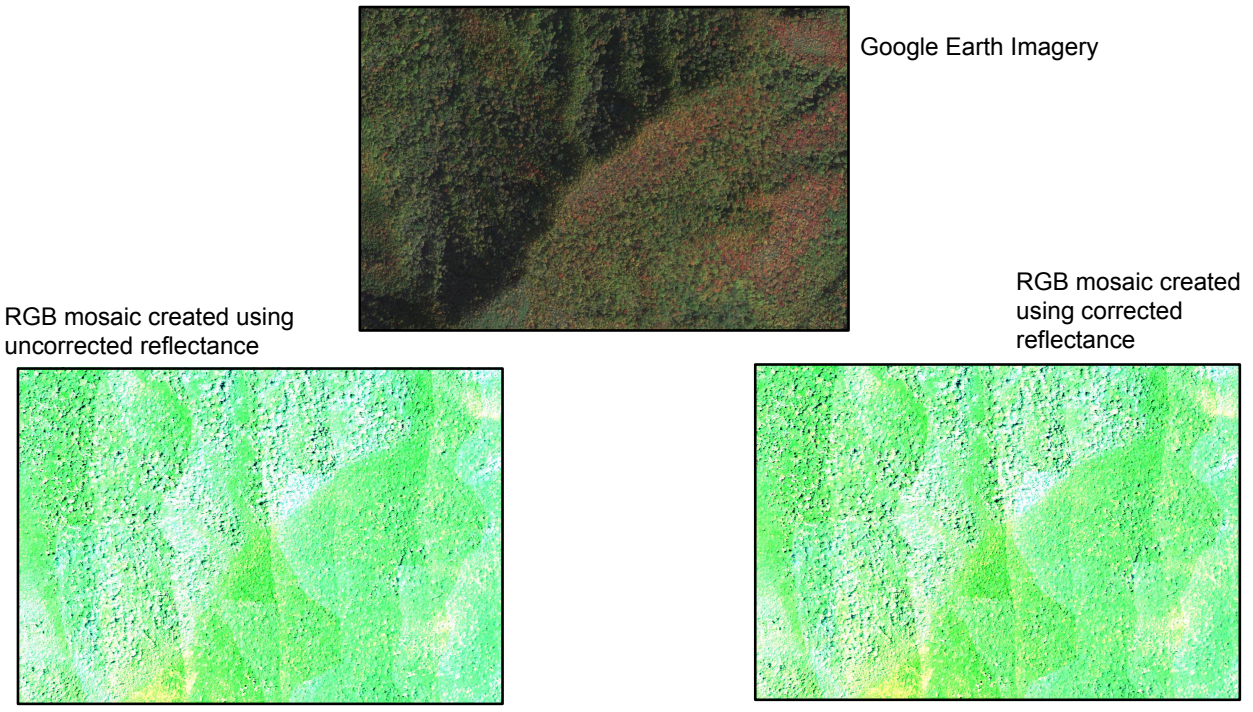

Figure 9: Topographic correction on the uncorrected reflectance for the GRSM site, TN did not significantly reduce the differences between reflectance values on either side of the ridge line.

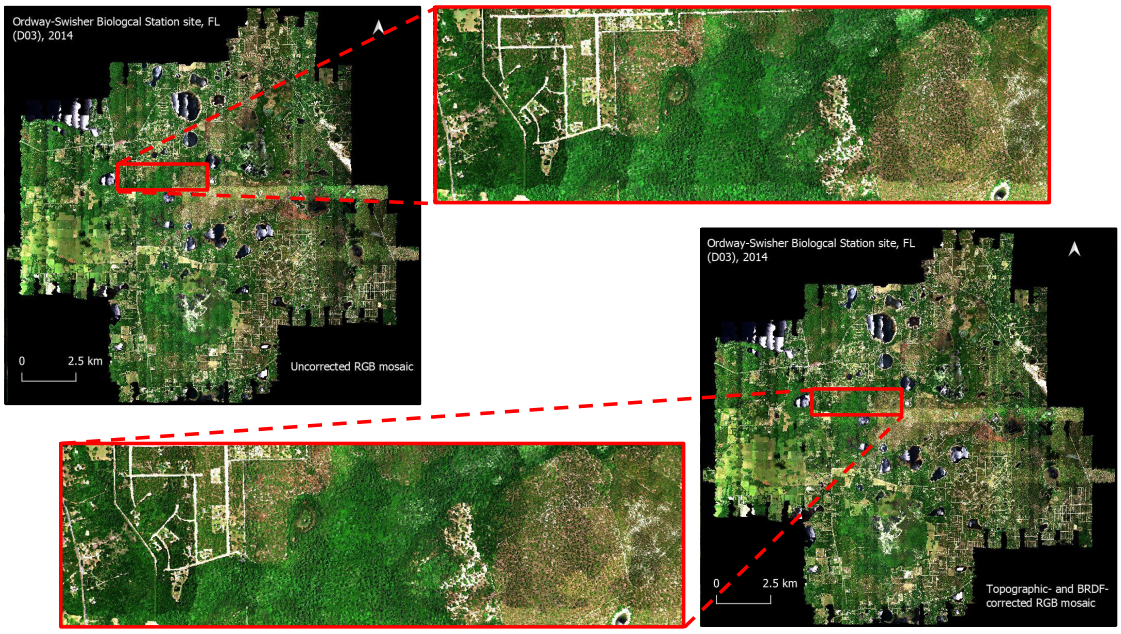

(a)

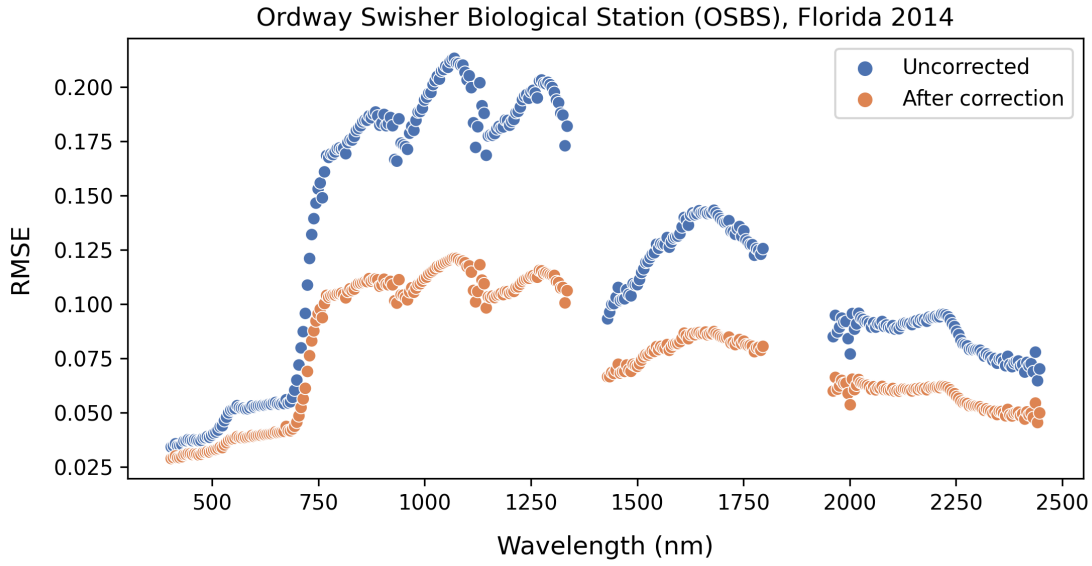

(b)

Figure 10: Results from applying topographic- and BRDF-corrections on the reflectance data from the OSBS site, FL **a)** Visual comparison on RGB mosaics before (left) and after (right) the correction **b)** A comparison of reflectance values between the overlapping areas of adjacent flight lines across all wavelength bands before and after applying the corrections. A lower value of RMSE indicates a closer match between overlapping areas, thus partially addressing the issue of brightness gradients. Some of the wavelength bands were dropped due to water vapor interference.

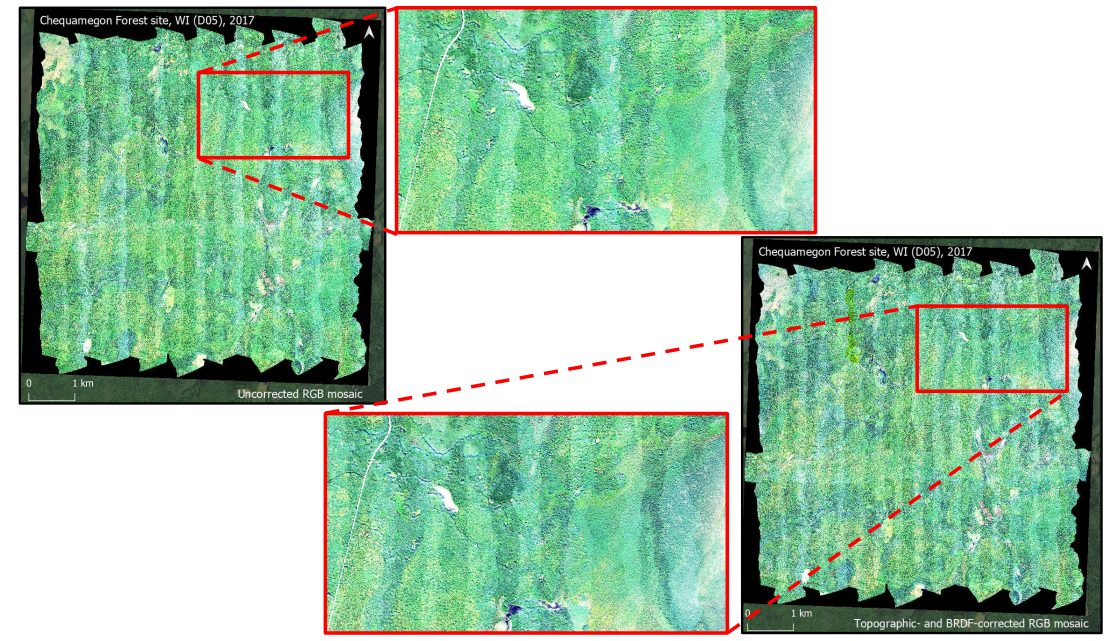

(a)

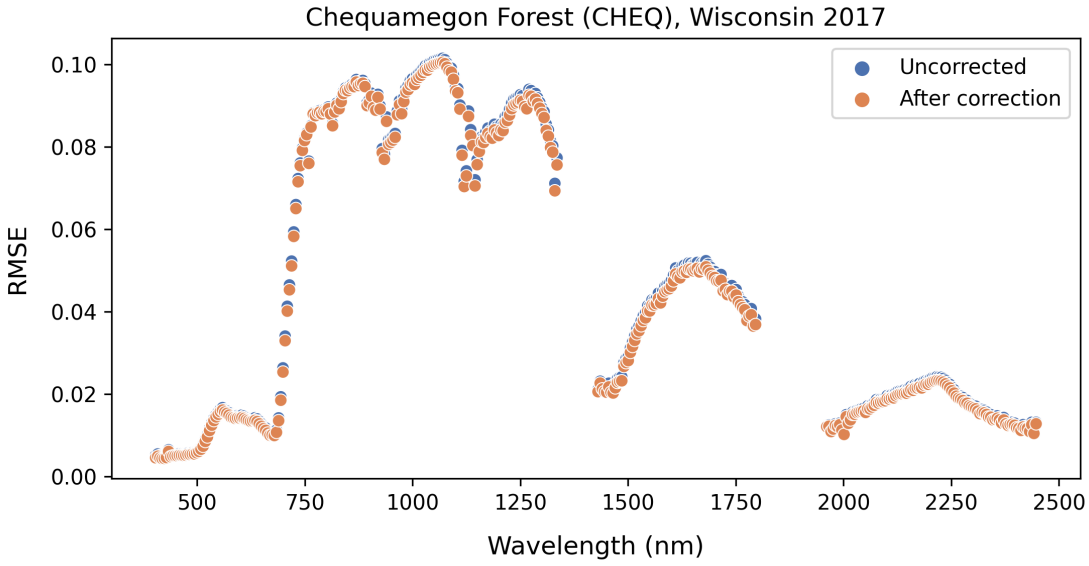

(b)

Figure 11: Results from applying topographic- and BRDF-corrections on the reflectance data from the CHEQ site, WI **a)** Visual comparison on RGB mosaics before (left) and after (right) the correction **b)** A comparison of reflectance values between the overlapping areas of adjacent flight lines across all wavelength bands before and after applying the corrections. A lower value of RMSE indicates a closer match between overlapping areas, thus partially addressing the issue of brightness gradients. Some of the wavelength bands were dropped due to water vapor interference.

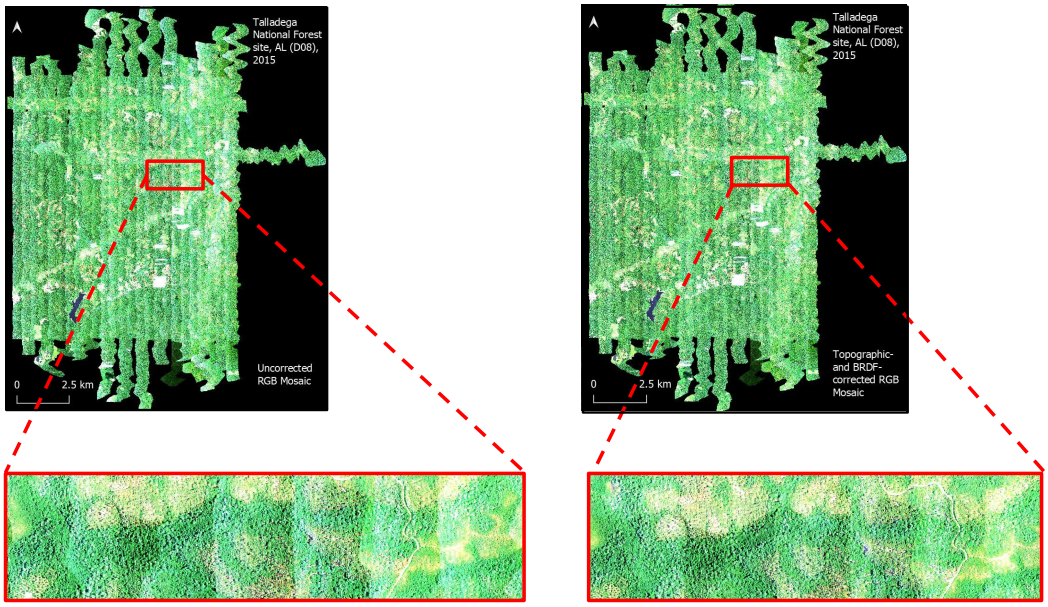

(a)

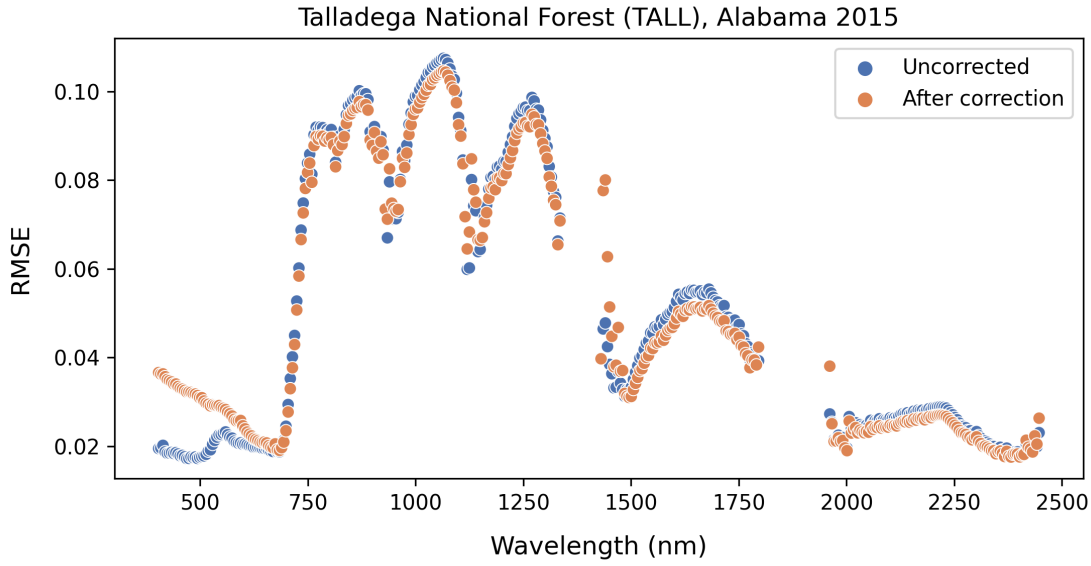

(b)

Figure 12: Results from applying topographic- and BRDF-corrections on the reflectance data from the TALL site, AL **a)** Visual comparison on RGB mosaics before (left) and after (right) the correction **b)** A comparison of reflectance values between the overlapping areas of adjacent flight lines across all wavelength bands before and after applying the corrections. A lower value of RMSE indicates a closer match between overlapping areas, thus partially addressing the issue of brightness gradients. Some of the wavelength bands were dropped due to water vapor interference.

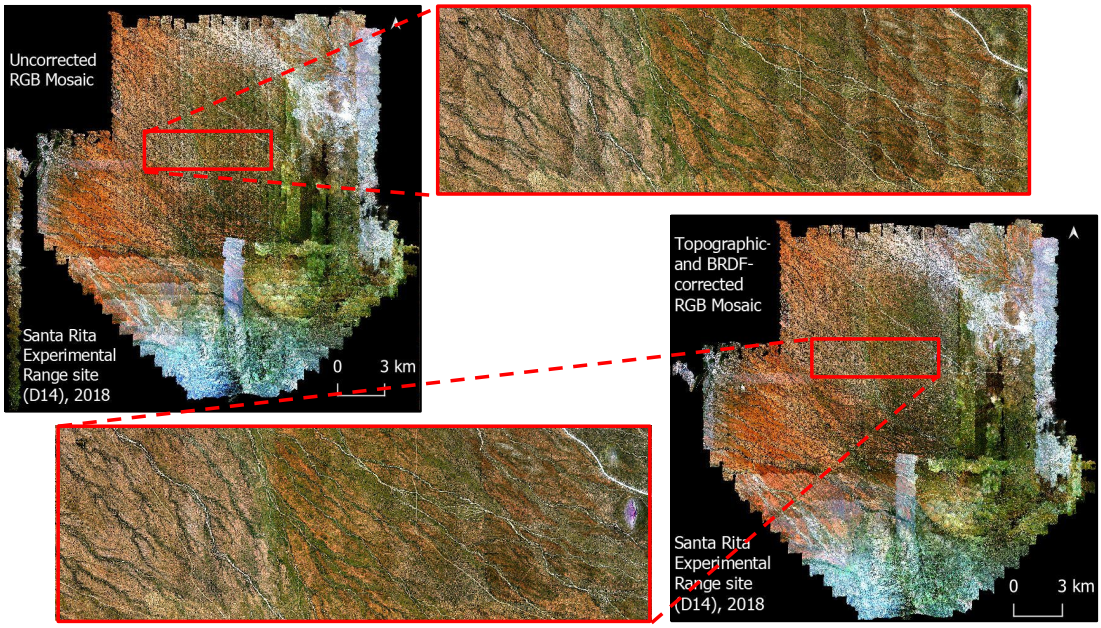

(a)

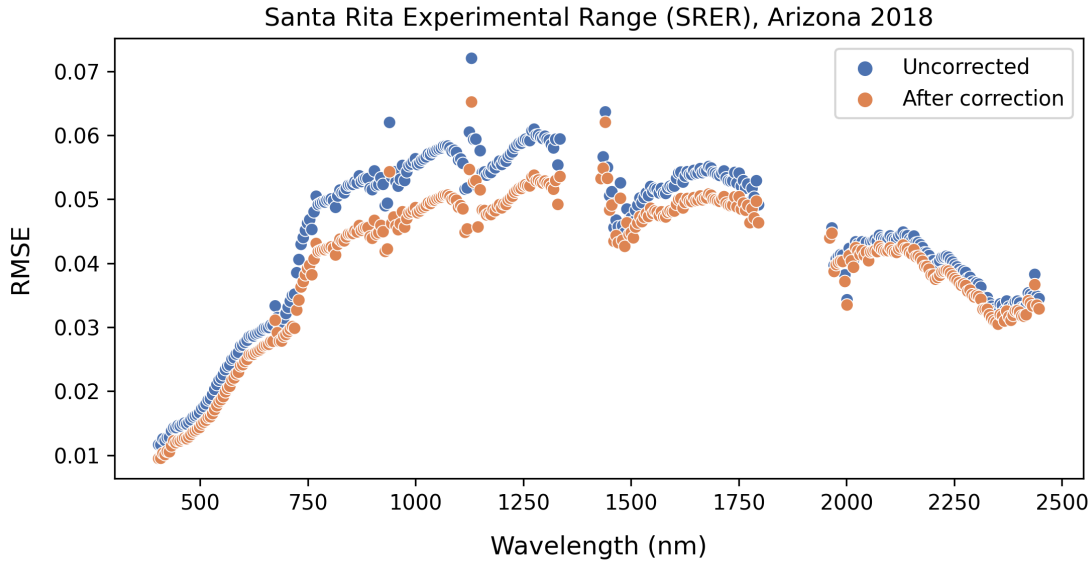

(b)

Figure 13: Results from applying topographic- and BRDF-corrections on the reflectance data from the SRER site, AZ **a)** Visual comparison on RGB mosaics before (left) and after (right) the correction **b)** A comparison of reflectance values between the overlapping areas of adjacent flight lines across all wavelength bands before and after applying the corrections. A lower value of RMSE indicates a closer match between overlapping areas, thus partially addressing the issue of brightness gradients. Some of the wavelength bands were dropped due to water vapor interference.

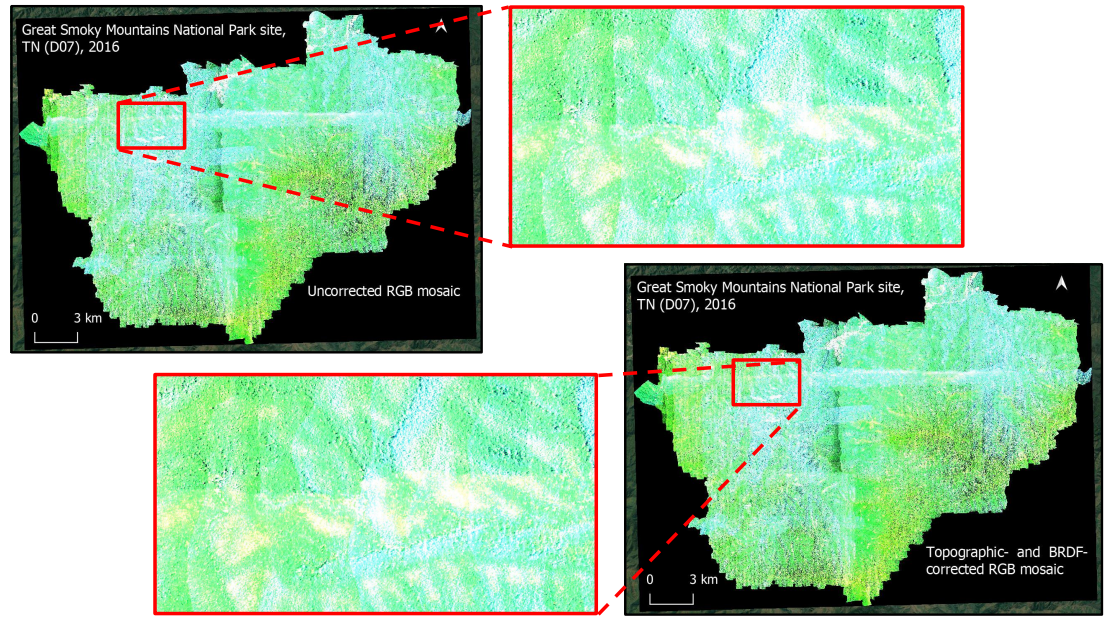

(a)

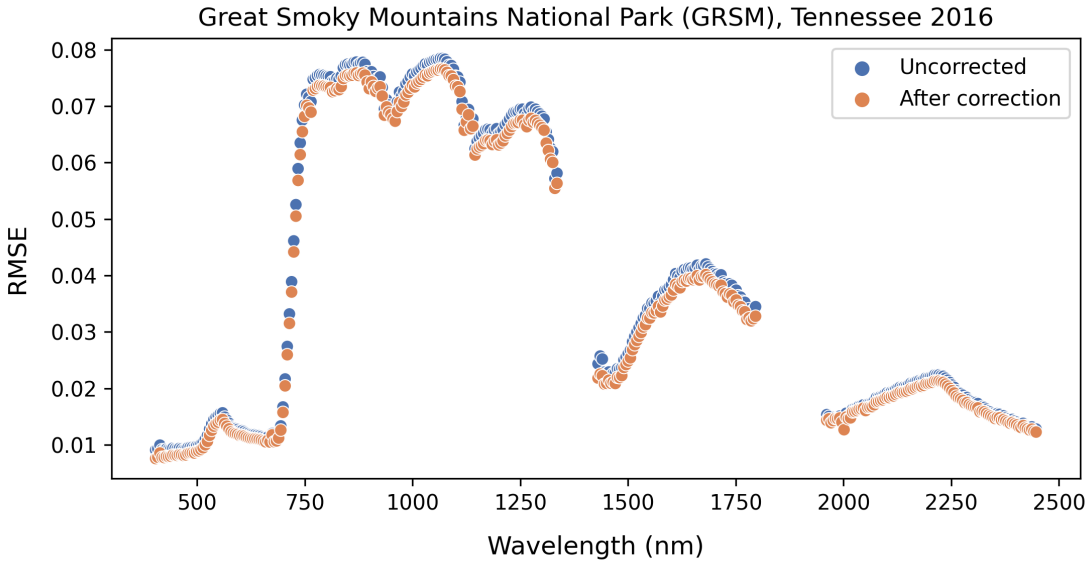

(b)

Figure 14: Results from applying topographic- and BRDF-corrections on the reflectance data from the GRSM site, TN **a)** Visual comparison on RGB mosaics before (left) and after (right) the correction **b)** A comparison of reflectance values between the overlapping areas of adjacent flight lines across all wavelength bands before and after applying the corrections. A lower value of RMSE indicates a closer match between overlapping areas, thus partially addressing the issue of brightness gradients. Some of the wavelength bands were dropped due to water vapor interference.

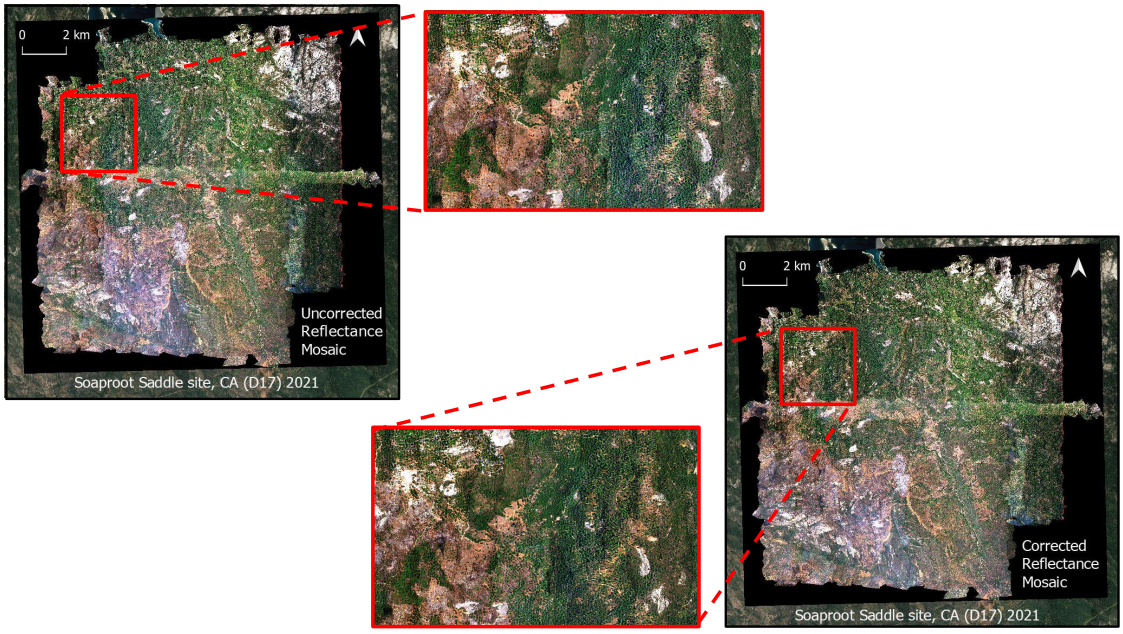

(a)

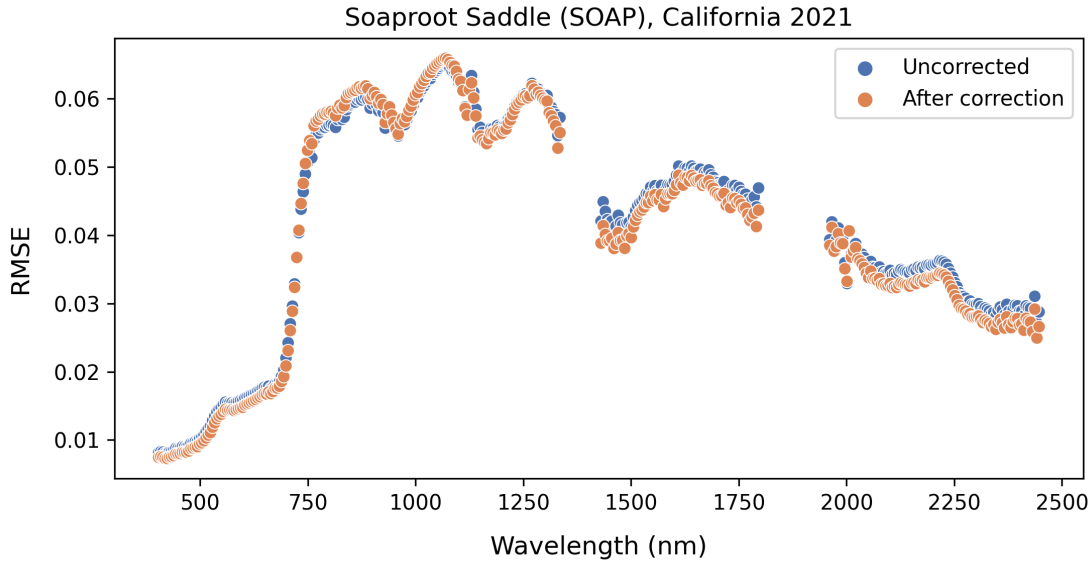

(b)

Figure 15: Results from applying topographic- and BRDF-corrections on the reflectance data from the SOAP site, CA **a)** Visual comparison on RGB mosaics before (left) and after (right) the correction **b)** A comparison of reflectance values between the overlapping areas of adjacent flight lines across all wavelength bands before and after applying the corrections. A lower value of RMSE indicates a closer match between overlapping areas, thus partially addressing the issue of brightness gradients. Some of the wavelength bands were dropped due to water vapor interference.

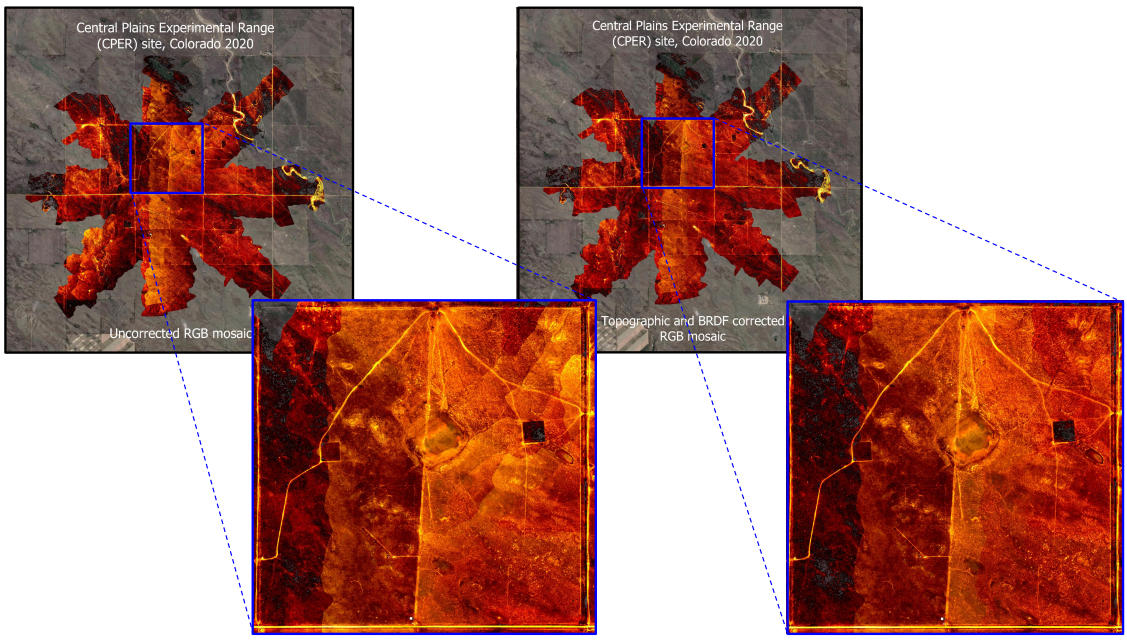

(a)

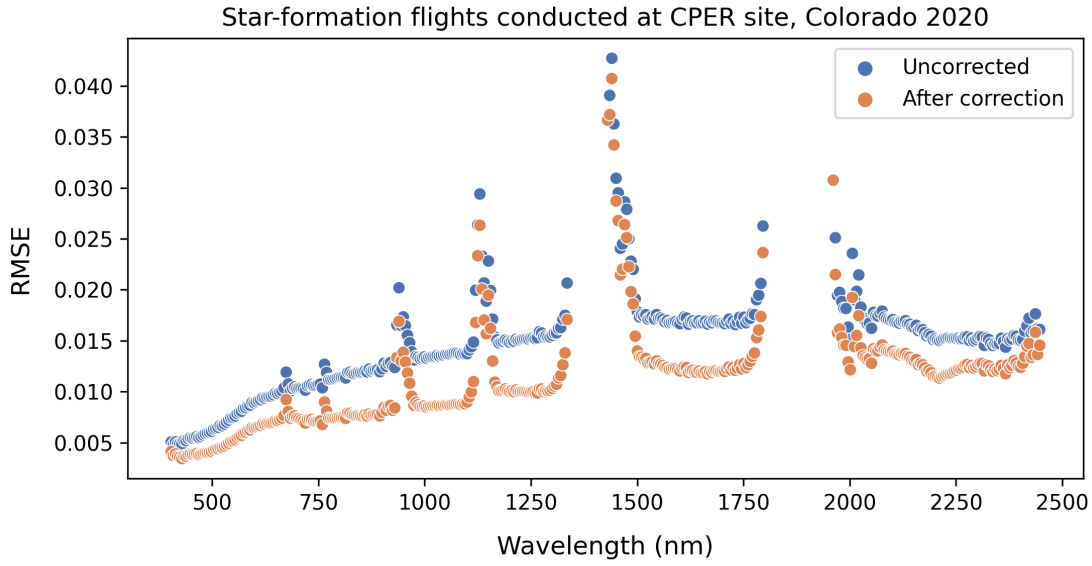

(b)

Figure 16: Results from applying topographic- and BRDF-corrections on the reflectance data from the CPER site, CO **a)** Visual comparison on RGB mosaics before (left) and after (right) the correction **b)** A comparison of reflectance values between the overlapping areas of adjacent flight lines across all wavelength bands before and after applying the corrections. A lower value of RMSE indicates a closer match between overlapping areas, thus partially addressing the issue of brightness gradients. Some of the wavelength bands were dropped due to water vapor interference.

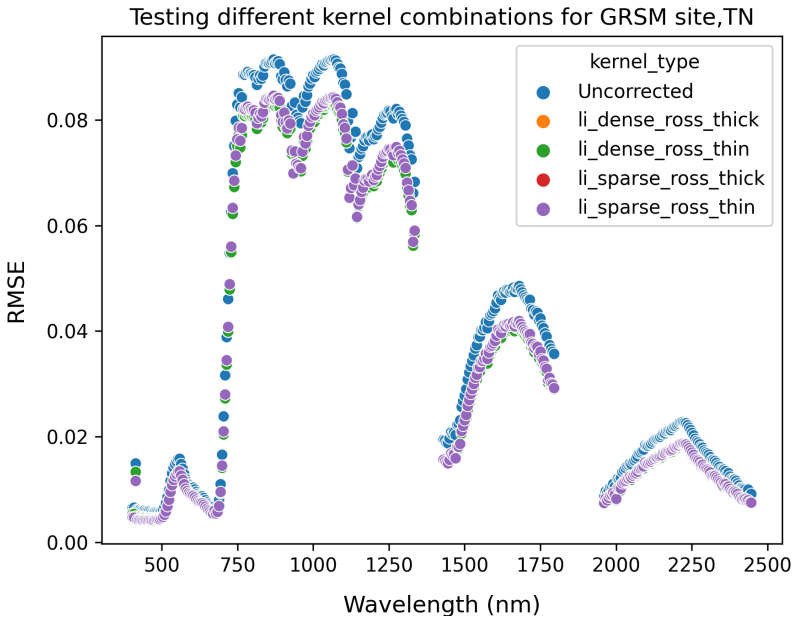

(a) Varying the kernel combinations did not improve the BRDF correction.

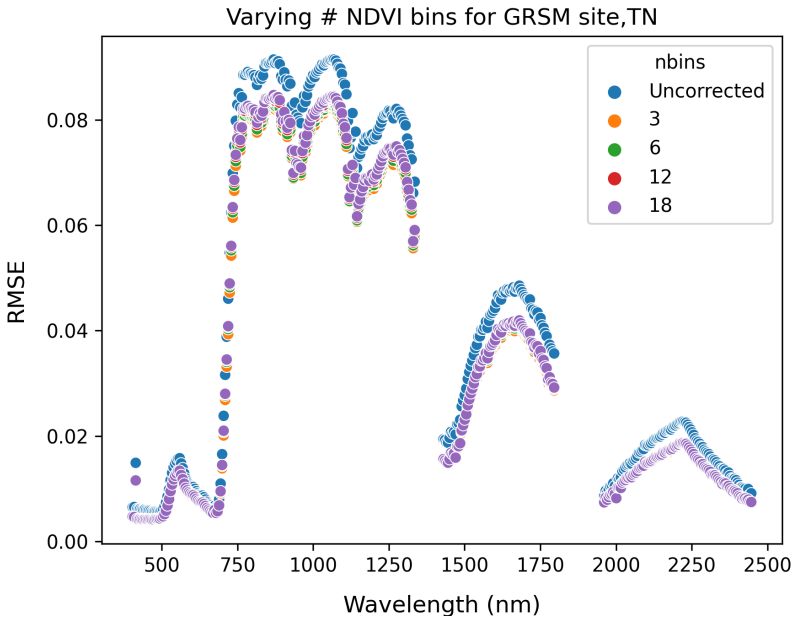

(b) Varying the number of NDVI bins did not improve the BRDF correction.

Figure 17: We varied the parameter values for BRDF correction for the GRSM site, TN, to identify the best values.

References

Colgan, M. S., Baldeck, C. A., Féret, J.-B., & Asner, G. P. (2012). Mapping savanna tree species at ecosystem scales using support vector machine classification and brdf correction on airborne hyperspectral and lidar data. *Remote Sensing*, *4*(11), 3462–3480. doi: https://doi.org/10.3390/rs4113462

Lucht, W., Schaaf, C., & Strahler, A. (2000). An algorithm for the retrieval of albedo from space using semiempirical brdf models. *IEEE Transactions on Geoscience and Remote Sensing*, *38*(2), 977-998. doi: 10.1109/36.841980

Musinsky, J., Goulden, T., Wirth, G., Leisso, N., Krause, K., Haynes, M., & Chapman, C. (2022). Spanning scales: The airborne spatial and temporal sampling design of the national ecological observatory network. *Methods in Ecology and Evolution*, *13*(9), 1866–1884.

National Ecological Observatory Network (NEON). (2023). *Spectrometer orthorectified surface directional reflectance - flightline (dp1.30006.001).* National Ecological Observatory Network (NEON). Retrieved from https://data.neonscience.org/data-products/DP1.30006.001/RELEASE-2023 doi: 10.48443/YPJZ-ET36

Queally, N., Ye, Z., Zheng, T., Chlus, A., Schneider, F., Pavlick, R. P., & Townsend, P. A. (2022). Flexbrdf: A flexible brdf correction for grouped processing of airborne imaging spectroscopy flightlines. *Journal of Geophysical Research: Biogeosciences*, *127*(1), e2021JG006622. doi: https://doi.org/10.1029/2021JG006622

Roujean, J.-L., Leroy, M., & Deschamps, P.-Y. (1992). A bidirectional reflectance model of the earth's surface for the correction of remote sensing data. *Journal of Geophysical Research: Atmospheres*, *97*(D18), 20455–20468. doi: https://doi.org/10.1029/92JD01411

Roy, D. P., Zhang, H., Ju, J., Gomez-Dans, J. L., Lewis, P. E., Schaaf, C., ... Kovalskyy, V. (2016). A general method to normalize landsat reflectance data to nadir brdf adjusted reflectance. *Remote Sensing of Environment*, *176*, 255–271. doi: https://doi.org/10.1016/j.rse.2016.01.023

Schaaf, C. B., Gao, F., Strahler, A. H., Lucht, W., Li, X., Tsang, T., ... others (2002). First operational brdf, albedo nadir reflectance products from modis. *Remote sensing of Environment*, *83*(1-2), 135–148. doi: https://doi.org/10.1016/S0034-4257(02)00091-3

Shepherd, J., & Dymond, J. (2003). Correcting satellite imagery for the variance of reflectance and illumination with topography. *International Journal of Remote Sensing*, *24*(17), 3503–3514.

Soenen, S., Peddle, D., & Coburn, C. (2005). Scs+c: a modified sun-canopy-sensor topographic correction in forested terrain. *IEEE Transactions on Geoscience and Remote Sensing*, *43*(9), 2148-2159. doi: 10.1109/TGRS.2005.852480

Wanner, W., Li, X., & Strahler, A. (1995). On the derivation of kernels for kernel-driven models of bidirectional reflectance. *Journal of Geophysical Research: Atmospheres*, *100*(D10), 21077–21089. doi: https://doi.org/10.1029/95JD02371